

# Accumulation and extraction of ultracold neutrons from a superfluid helium converter coated with fluorinated grease

O. Zimmer<sup>1,2\*</sup>, P. Schmidt-Wellenburg<sup>1,2</sup>, M. Assmann<sup>1</sup>, M. Fertl<sup>1</sup>,  
J. Klenke<sup>3</sup>, S. Mironov<sup>1,4</sup>, H.-F. Wirth<sup>1</sup>, B. van den Brandt<sup>5</sup>

<sup>1</sup>Physik-Department E18, Technische Universität München,  
D-85748 Garching, Germany

<sup>2</sup>Institut Laue-Langevin, B.P. 156, 38042 Grenoble, France

<sup>3</sup>Forschungsreaktor München FRM II, Lichtenbergstrasse 1, 85747 Garching, Germany

<sup>4</sup>Laboratory of Nuclear Problems, JINR, Dubna, Moscow region 141980, Russia

<sup>5</sup>Paul Scherrer Institut, CH-5232 Villigen PSI, Switzerland

August 9, 2021

## Abstract

We report experiments on the production of ultracold neutrons (UCN) in a converter of superfluid helium coated with fluorinated grease. We employed our technique of window-free extraction of accumulated UCN from the helium, in which they were produced by downscattering neutrons of a cold beam from the Munich research reactor. The time constant for UCN passage through the same extraction aperture as in a previous experiment was a factor two shorter, despite a lower mean velocity of the accumulated UCN in the present experiments. A time-of-flight measurement of the cold neutron spectrum incident on the converter allowed us to estimate the multi-phonon contribution to the UCN production. The UCN production rate inferred from two methods agrees with the theoretical expectation.

PACS numbers: 78.70.Nx, 28.20.Fc, 29.25.Dz, 61.12.Ha

Keywords: ultracold neutrons, UCN, UCN sources

\*email: zimmer@ill.fr

## 1 Introduction

Ultracold neutrons (UCN) have energies in the neV range and velocities up to a few meters per second. When impinging on suitable materials they undergo total reflection under any angle of incidence and can therefore be trapped in bottles and manipulated for a long time (see the books [1, 2] for an introduction to the physics of UCN). Owing to this feature UCN have become very useful in various fundamental investigations of neutron properties, with strong implications for particle physics and cosmology. The longstanding search for the neutron electric dipole moment investigates CP-violation beyond the standard model of particle physics [3, 4]. The accurate determination of the neutron lifetime is required for a detailed understanding of big bang nucleosynthesis [5], and to investigate strength and structure of the semi-leptonic weak interaction within the first quark family (see, e.g., the workshop proceedings [6, 7]). New topics with UCN are, among others, the demonstration of quantum levels of neutrons in the earth's gravitational field [8], and even more recently, the search for neutron - mirror neutron transitions [9, 10]. The most intense UCN source at the Institut Laue Langevin in Grenoble [11] provides

33 not more than 50 UCN per  $\text{cm}^3$ . In order to improve counting statistics, new UCN sources are  
34 being developed in many laboratories around the world [12, 13, 14, 15, 16, 17, 18].

35 An elegant method to produce UCN employs a converter of superfluid  $^4\text{He}$  in a beam of cold  
36 neutrons [19]. The kinematics defined by the dispersion relations of helium and the free neutron  
37 enables downscattering of cold neutrons with an energy around 1.0 meV (wavelength 0.89 nm)  
38 to ultracold energies via emission of a single phonon. In addition, multi-phonon processes occur  
39 which contribute to the integral UCN production rate for a wide range of incident neutron  
40 energies [20, 21]. At low temperatures the probability for upscattering is strongly suppressed by  
41 the Boltzmann factor. Therefore, and since pure  $^4\text{He}$  has no cross section for neutron absorption,  
42 a large density of UCN may build up in a converter with reflective walls. The storage time  
43 constant  $\tau$  can of course not exceed a limit close to 900 s set by the neutron beta decay lifetime.

44 In a recent experiment we have demonstrated for the first time that one may efficiently extract  
45 UCN from the converter after having them accumulated therein [22]. As in past experiments  
46 [16, 17, 23, 24] the UCN production rate was found to agree reasonably well with the theoretical  
47 expectation. We have developed a new cryostat designed to keep the source portable and easy  
48 to operate. With a short cooling cycle of a few days, our system is much more flexible than  
49 an earlier apparatus [25], which was designed to be installed close to the target of a spallation  
50 source. Our present apparatus is a prototype for a future UCN source to be installed at a strong  
51 cold neutron beam of a high-flux reactor, where no extraordinary cooling power is required.  
52 A particular feature is the vertical extraction of the UCN through a cold mechanical valve  
53 situated above the helium bath. In contrast to a previous attempt to extract accumulated UCN  
54 horizontally [26], no gaps or windows are required in our method. To gain first experience with  
55 this system, the UCN converter vessel and extraction guide system were made of stainless steel.  
56 In the first run it enabled us to measure, with negligible background, the UCN production rate  
57 and to study the temperature-dependent storage properties of the converter. Here we report  
58 new results obtained with the converter vessel coated with fluorinated grease (Fomblin). It has  
59 good reflection properties for UCN and, to our very surprise, positively influences the extraction  
60 time constant. Moreover, a time-of-flight (TOF) measurement of the incident cold neutron beam  
61 helped to improve the comparison with the theoretical UCN production rate.

## 62 2 Apparatus

63 The apparatus was already described in some detail in ref. [22]. The converter vessel has a  
64 volume of about 2.4 liters, made from an electropolished stainless steel tube with length 696  
65 mm and inner diameter 66 mm, closed by Ni windows on both ends. The lowest temperature  
66 attained for the completely filled vessel was  $T = 0.72$  K in the previous run, and 0.82 K in the  
67 present. The maximum kinetic energy of UCN storable in the vessel is defined by the Fermi  
68 potential  $V_{\text{F,wall}}$  of the wall material, which is  $(184 \pm 4)$  neV for the stainless steel used (and 252  
69 neV for the Ni windows), from which one has to subtract the Fermi potential of the superfluid  
70 helium ( $V_{\text{F},^4\text{He}} = 18.5$  neV). Due to a small neutron absorbing aperture with diameter 33 mm  
71 placed at the entrance window to the converter, chosen in order to avoid activation of the  
72 vessel in these first test experiments, the volume intersected by the cold neutron beam ("UCN  
73 production volume") was  $V_{\text{p}} = 595$   $\text{cm}^3$ , only. In the experiments reported here, the inner  
74 surface of the vessel was coated with a thick layer of fluorinated grease (Fomblin) with a Fermi  
75 potential of  $(115 \pm 10)$  neV. UCN were extracted as previously through a flapper valve situated  
76 above the superfluid helium in the "T" section of the storage tube, connecting the (uncoated)  
77 extraction line made of electropolished stainless steel to a  $^3\text{He}$ -gas UCN detector. The present  
78 experiments were again performed at the neutron guide "NL1" at the Munich research reactor  
79 FRM II, using the same neutron beam collimation as in the previous setup [22].

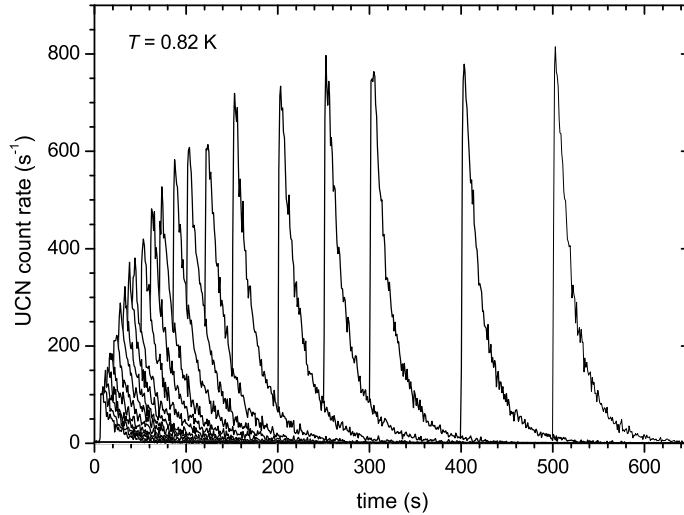


**Figure 1:** Time histograms of UCN count rates, measured in "buildup mode" (see text) at 0.82 K for 23 different accumulation times  $t_0$ .

### 3 Definition of time constants and measurements

UCN storage and extraction from the converter can be characterised by various time constants. The storage time constant  $\tau$  quantifies the temporal decrease of UCN in the closed vessel. The rate  $\tau^{-1}$  contains a contribution  $\tau_0^{-1}$  due to wall collisions, absorbing impurities, and UCN escaping through small holes in the vessel. This contribution does not depend on temperature  $T$  but on the kinetic energy  $E$  of the UCN. In addition there are the rates for the  $T$ -dependent UCN upscattering, and for neutron beta decay<sup>1</sup>,

$$\tau^{-1} = \tau_0^{-1}(E) + \tau_{\text{up}}^{-1}(T) + \tau_{\beta}^{-1}. \quad (1)$$

The emptying time constant  $\tau_e$  quantifies the temporal decrease of UCN in the vessel with the UCN valve open. Therefore,

$$\tau_e^{-1}(T, E) = \tau^{-1}(T, E) + \tau_A^{-1}(E), \quad (2)$$

where  $\tau_A$  is the time constant for UCN passage through the extraction hole with area  $A$ . From these time constants we may derive the detection probability  $W$  for a UCN created in the converter vessel. It characterises the efficiency of the whole system including extraction and is given by

$$W = \varepsilon \frac{\tau_A^{-1}}{\tau_e^{-1}} = \varepsilon \frac{\tau - \tau_e}{\tau}, \quad (3)$$

where the factor  $\varepsilon$  describes losses in the extraction line and imperfect detector efficiency. The conversion process employed in the present experiments produces a broad spectrum of low-energy neutrons. Only neutrons with energies below  $V_{\text{F,wall}} - V_{\text{F},^4\text{He}}$  are trapped inside the converter vessel, whereas those with higher energies quickly escape. The spectrum of the neutrons remaining in the vessel is shaped due to wall losses. The energy dependence of these losses is

<sup>1</sup>In the present experiments this contribution forgotten to mention in ref. [22] was still small compared to the sum of the other rates.

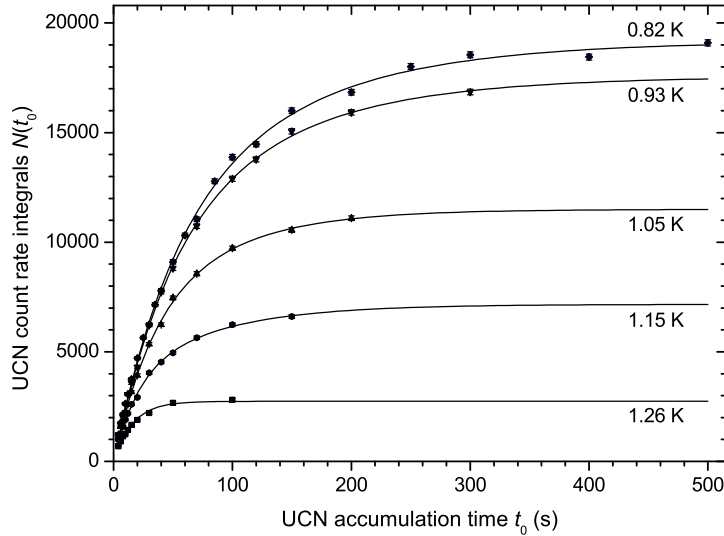


**Figure 2:** UCN count rate integrals as a function of the accumulation time  $t_0$ . The fit to the data points at  $T = 1.26$  K is performed with the single-exponential function defined in eq.(4). The results for the fitting parameters  $\tau$  and  $N$  are employed in section 4 to determine the UCN production rate. The fits to the data points for lower temperatures employ double exponentials and serve as guides to the eye.

98 due to the increase with UCN energy of both the average loss probability per wall collision and  
 99 the frequency of wall collisions. Thus the largest losses occur for those neutrons with energies  
 100 close to the Fermi potential. However, if on a given time scale the change of the energy spec-  
 101 trum stays sufficiently small, the time constant  $\tau$  is still well defined. This is found to be a  
 102 reasonably good approximation for the accumulation of UCN at high temperatures, where the  
 103 energy-independent  $\tau_{\text{up}}^{-1}(T)$  dominates the rate  $\tau^{-1}$  (see eq.(1)). At lower temperatures we may  
 104 still deduce values for the various  $\tau$ s (still calling them "time constants"), and study how they  
 105 depend on the times of UCN accumulation and trapping.

106 The time constants  $\tau$  and  $\tau_e$  can be obtained from measurements in the "buildup mode".  
 107 There, the closed converter is first irradiated with cold neutrons for a time  $t_0$ , after which the  
 108 beam is shut off and simultaneously the UCN valve is opened. During the whole process a time  
 109 histogram of the UCN count rate is recorded. Figure 1 shows a series of such histograms for  
 110 different accumulation times  $t_0$ , which was obtained for the lowest temperature of the converter  
 111 in the present runs. The decrease of the UCN count rate while emptying the vessel proceeds with  
 112 a pure single-exponential; fits of the whole decay in each of the histograms with  $A \exp(-t/\tau_e)$   
 113 always resulted in a reduced  $\chi^2$  close to unity and provided a value for  $\tau_e$  for each of the  
 114 histograms.

115 Figure 2 shows the integrals  $N(t_0)$  of all histograms measured. It demonstrates the satura-  
 116 tion behaviour and the strong  $T$  dependence of UCN accumulation for the range of temperatures  
 117 investigated. If the time constant  $\tau$  is sufficiently well defined, one can fit to the data the single-  
 118 exponential buildup function

$$N(t_0) = N(1 - \exp(-t_0/\tau)). \quad (4)$$

119 For the highest temperature,  $T = 1.26$  K, this fit has a reduced  $\chi^2$  of 3.5. The fit becomes

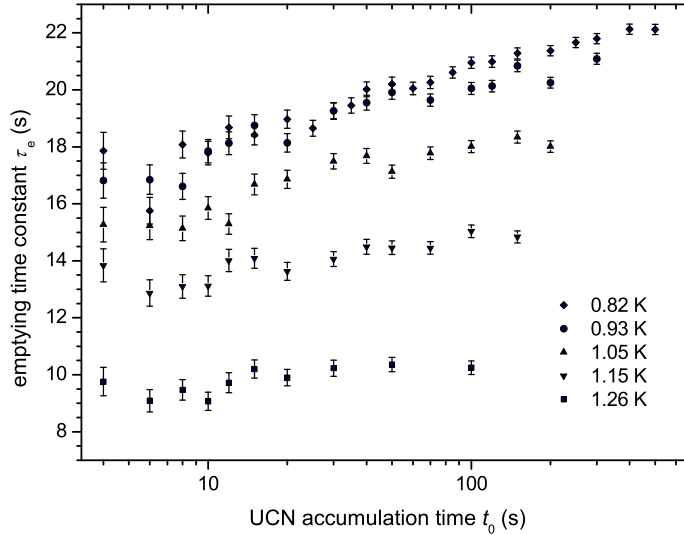


**Figure 3:** Emptying time constants  $\tau_e$  as a function of the UCN accumulation time  $t_0$ , determined from the histograms of all buildup-mode measurements for the various converter temperatures.

120 increasingly worse for the lower temperatures. As visible in fig. 3, there is also a dependence of  
 121  $\tau_e$  on  $t_0$ , which becomes increasingly pronounced for lower temperatures. These facts indicate  
 122 the increasing influence of the first term in eq.(1) with decreasing temperature. The fit of a  
 123 constant value to the data for  $\tau_e$  at 1.26 K has  $\chi^2 = 2.3$ . For later use we summarise below the  
 124 results of the fits to the data at this temperature, and the corresponding value for  $\tau_A$ , obtained  
 125 with eq.(2) and the value for  $\tau$  from eq.(5). The uncertainties stated for  $\tau$ ,  $N$ , and  $\tau_e$  have been  
 126 scaled to provide a fit with  $\chi^2 = 1$ :

$$\begin{aligned}
 \tau &= (15.79 \pm 0.82) \text{ s}, \\
 N &= 2740 \pm 73, \\
 \tau_e &= (9.92 \pm 0.15) \text{ s}, \\
 \tau_A &= (26.7 \pm 2.6) \text{ s}.
 \end{aligned}
 \tag{5}$$

127 From the buildup-mode measurements as described before we cannot extract values for  $\tau$   
 128 as a function of the time the UCN stay trapped in the vessel. In order to demonstrate this  
 129 dependence we employed a variant of such measurements with a delayed extraction. There  
 130 again the converter is first irradiated with cold neutrons while the UCN valve stays closed.  
 131 After an accumulation time  $t_0$  the beam is shut, but the UCN valve is opened only after a  
 132 delay time  $t_d$ . A series of such measurements provides histograms for the same  $t_0$  but various  
 133  $t_d$ . A plot of the count rate integrals of two series, for  $t_0 = 25$  s and 250 s, is shown in fig. 4.  
 134 Values for  $\tau$  can be obtained from single-exponential fits to a group of several data points. The  
 135 variation of slope of the curves shown in fig. 4 indicates a more pronounced increase of  $\tau$  with  
 136  $t_d$  when UCN are accumulated for a longer time. This is to be expected, since after  $t_0 = 250$  s  
 137 the relative abundance of slower UCN with respect to the (more abundant) faster ones will be  
 138 significantly higher than after 25 s, due to the longer storage time constant of the slower UCN.  
 139 Their presence in the vessel then becomes better visible in the delayed-extraction experiments.

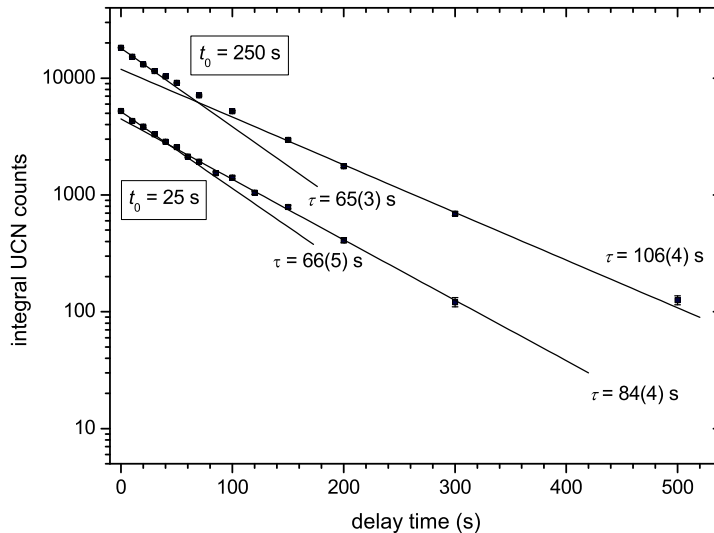


**Figure 4:** Count rate integrals of the measurements at 0.82 K with delayed extraction after UCN accumulation times  $t_0 = 25$  s (lower data points) and 250 s (upper data points). The solid lines are fits of single exponentials to the four first, respectively, four last data points. The corresponding time constants  $\tau$  derived from these fits are also shown.

$T$ [K]	1.26	1.15	1.05	0.93	0.82
$\dot{N}_c$ [ $s^{-1}$ ]	$176 \pm 2.6$	$227.6 \pm 2.7$	$257.5 \pm 1.4$	$278.3 \pm 2.3$	$286.6 \pm 1.6$
$W/\varepsilon$ [%]	$37.1 \pm 3.4$	48.0	54.3	58.7	60.4

**Table 1:** Measured  $T$ -dependent count rates obtained in continuous-mode measurements, and values deduced for  $W/\varepsilon$  (see text).

140 Values for  $\tau$  can also be deduced from the integral UCN counts for only two different delay  
 141 times, using the relation

$$\tau = \frac{t_{d_2} - t_{d_1}}{\ln N(t_{d_1}) - \ln N(t_{d_2})}. \quad (6)$$

142 Figure 5 shows such an analysis for the series with  $t_0 = 250$  s. The strong variation of time  
 143 constants from one to two minutes demonstrates indeed how much at 0.82 K the spectrum of the  
 144 UCN remaining in the vessel is shaped by the energy dependence of the wall collisions during  
 145 trapping.

146 In a third type of measurements, called "continuous mode", we measured the steady state  
 147 count rate  $\dot{N}_c$  with the converter irradiated for a long time with cold neutrons while the  
 148 UCN valve stayed open. The count rates measured are listed in Table 1. In the next section  
 149 we will use  $\dot{N}_c$  and  $W/\varepsilon$  at 1.26 K as input to determine the UCN production rate. For  
 150 the purpose of illustration we present in Table 1 also values for  $W/\varepsilon$  derived from  $W(T_i) =$   
 151  $W(1.26 \text{ K})\dot{N}_c(T_i)/\dot{N}_c(1.26 \text{ K})$ , which assumes that the same UCN spectrum prevails for the dif-  
 152 ferent temperatures. Remember that, as obvious from fig. 3, this assumption is only valid as  
 153 an approximation. The values stated for the lower temperatures might represent the true value  
 154 with a relative error in the order of 10 %.

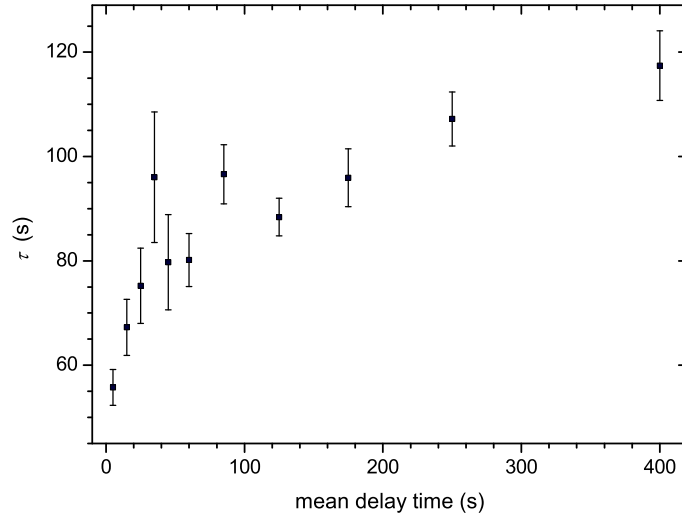


**Figure 5:** UCN storage time constants deduced from eq.(6), using adjacent data points from the measurements with delayed extraction shown in fig. 4. The abscissa is given by the mean of the two adjacent delay times,  $(t_{d_{i+1}} + t_{d_i})/2$ .

## 4 UCN production rate

The UCN production rate can be inferred from two methods, for which we employ the data at the highest temperature,  $T = 1.26$  K, where the time constants are sufficiently well defined.

First, as in the analysis of our last experiments [22], we may use the stationary "continuous mode" count rate  $\dot{N}_c$ . The corresponding UCN production rate density  $P_1$  is given by

$$P_1 = \frac{\dot{N}_c}{V_p W}. \quad (7)$$

Using the values for  $\dot{N}_c$  and  $W/\varepsilon$  stated in Table 1 and the value  $V_p = 595$  cm<sup>3</sup> for the UCN production volume, we obtain

$$\varepsilon P_1 = (0.797 \pm 0.074) \text{ s}^{-1} \text{ cm}^{-3}. \quad (8)$$

Lacking the knowledge of  $\varepsilon$ , the numerical value in eq.(8) provides a lower limit for  $P_1$ .

A second value for the production rate density,  $P_2$ , may be derived from the saturated UCN number  $N$  in the buildup-mode measurement, employing eq.(4). When UCN are accumulated for a long time,  $t_0 \gg \tau$ , the production rate equals the UCN loss rate. Denoting with  $N_0$  the saturated number of UCN in the vessel, of which only the fraction  $N = N_0 W$  is detected, this leads us to

$$P_2 = \frac{N}{W V_p \tau}. \quad (9)$$

Using the values for  $\tau$  and  $N$  from eq.(5) with  $W/\varepsilon$  from Table 1 we obtain

$$\varepsilon P_2 = (0.786 \pm 0.085) \text{ s}^{-1} \text{ cm}^{-3}. \quad (10)$$

Hence, within the 10 % accuracy of these two methods,  $P_1 = P_2$ . We may now compare the experimental findings with the theoretical expectation. This requires knowledge of the incident

171 cold neutron spectrum which we measured in a separate experiment, using a time-of-flight (TOF)  
 172 analysing device described in ref. [27]. It consists of a mechanical chopper and a  $^3\text{He}$  detector  
 173 with a vertical slit. During a measurement the detector was moved horizontally in order to  
 174 integrate over the whole divergence of the beam. The entrance aperture of the TOF analyser  
 175 was placed at the position where previously was situated the entrance window to the converter  
 176 vessel. We thus determined the neutron wavelength spectrum up to  $\lambda = 2$  nm (frame overlap of  
 177 the chopped bunches occurred only for  $\lambda > 5$  nm, where the intensity is negligibly small). The  
 178 part for  $\lambda \leq 1$  nm is shown in fig. 6. After the TOF measurements the spectrum was calibrated  
 179 with a gold foil activation by the integral neutron flux.

180 The mechanism of UCN production contains contributions from single phonon emission and  
 181 multiphonon processes. The single-phonon contribution to the production rate density in a  
 182 helium converter with Be wall coating is  $P_I = (4.55 \pm 0.25) \times 10^{-9} \text{ d}\phi/\text{d}\lambda|_{\lambda^*} \text{ s}^{-1}\text{cm}^{-3}$ , where  
 183 the differential flux at  $\lambda^* = 0.89$  nm is given in  $\text{cm}^{-2}\text{s}^{-1}\text{nm}^{-1}$  [17]. For the present situation  
 184 this value needs to be corrected for the Fermi potential of the Fomblin grease, i.e. divided by  
 185  $(252 - 18.5)^{3/2} / (115 - 18.5)^{3/2} = 3.76$ , with an uncertainty of 0.59 due to the poor knowledge  
 186 of the Fermi potential of the Fomblin grease. From the measured TOF spectrum shown in fig. 6a  
 187 we find  $\text{d}\phi/\text{d}\lambda|_{\lambda^*} = 5.0 \times 10^8 \text{ cm}^{-2}\text{s}^{-1}\text{nm}^{-1}$ , from which we expect a single-phonon production  
 188 rate density  $P_I = (0.61 \pm 0.10) \text{ s}^{-1}\text{cm}^{-3}$ .

189 The differential multi-phonon production rate density is given by

$$\frac{\text{d}P_{\text{II}}}{\text{d}\lambda} = n_{4\text{He}}\sigma_{4\text{He}}E_c \frac{k_c}{3\pi} \frac{\text{d}\phi}{\text{d}\lambda} s_{\text{II}}(\lambda)\lambda. \quad (11)$$

190  $n_{4\text{He}}$  is the number density and  $\sigma_{4\text{He}}$  is the cross section per helium atom.  $E_c$  and  $k_c$   
 191 are the maximum kinetic energy and wavenumber of the neutrons trapped in the vessel.  $s_{\text{II}}(\lambda)$   
 192 is the scattering function  $s_{\text{II}}(Q, \omega)$ , evaluated on the dispersion curve of the free neutron, i.e.  
 193  $\omega = \hbar Q^2/(2m_n)$ , with  $Q = 2\pi/\lambda$ . It is modeled<sup>2</sup> to fit data from [28, 29] which is also shown  
 194 in fig. 6a. Integration of  $\text{d}P_{\text{II}}/\text{d}\lambda$  from 0.52 nm to  $\infty$  for the measured incident differential flux  
 195 provides an estimated lower limit of  $0.42 \text{ s}^{-1}\text{cm}^{-3}$  for the integral multi-phonon production rate  
 196  $P_{\text{II}}$ . Difficult to estimate is the contribution to  $P_{\text{II}}$  from the wavelength range  $\lambda < 0.52$  nm.  
 197 First, there is no direct experimental information available about  $s_{\text{II}}(\lambda)$  and second, this region  
 198 has a strong weight due to the relatively large  $\text{d}\phi/\text{d}\lambda$ . The  $\lambda$ -dependent measurements of UCN  
 199 production by Baker and colleagues [17] indicate that a multi-phonon contribution exists also  
 200 from the region  $0.4 \text{ nm} \leq \lambda \leq 0.52 \text{ nm}$ . The measured integral multi-phonon and single-phonon  
 201 production rates were found to add up evenly to the measured integral production rate [30].  
 202 This provides an experimental hint that for  $\lambda < 0.4$  nm the multi-phonon contribution might  
 203 be negligible. The fit function shown in fig. 6 was therefore designed to extend the range of  
 204 available data with a smooth decrease to zero at 0.4 nm. Integration of  $\text{d}P_{\text{II}}/\text{d}\lambda$  using the  
 205 complete fitting function for  $s_{\text{II}}(\lambda)$  yields  $P_{\text{II}} = 0.56 \text{ s}^{-1}\text{cm}^{-3}$ . Estimating the uncertainty of  
 206  $P_{\text{II}}$  as the difference between the values with and without inclusion of the contribution from the  
 207 range  $0.4 \text{ nm} \leq \lambda \leq 0.52 \text{ nm}$ , we may expect a total UCN production rate of

$$P_{\text{th}} = (0.61 \pm 0.10)_I \text{ s}^{-1}\text{cm}^{-3} + (0.56 \pm 0.14)_{\text{II}} \text{ s}^{-1}\text{cm}^{-3} = (1.17 \pm 0.17) \text{ s}^{-1}\text{cm}^{-3}. \quad (12)$$

208 Evidently, more experimental information about  $s_{\text{II}}(\lambda)$  is required for a secure prediction of  
 209 the UCN production rate induced by a white cold neutron beam. Note that this is particularly  
 210 necessary for the region of short wavelengths, whereas the contribution to  $P_{\text{II}}$  from the region  
 211  $\lambda > 0.8$  nm is only  $0.03 \text{ s}^{-1}\text{cm}^{-3}$ . We also note that predictions from the two model calculations  
 212 [20, 21] for the region  $\lambda < 0.52$  nm give mutually inconsistent results.

<sup>2</sup>More details about the modeling of  $s_{\text{II}}(\lambda)$  will be described in a forthcoming paper.



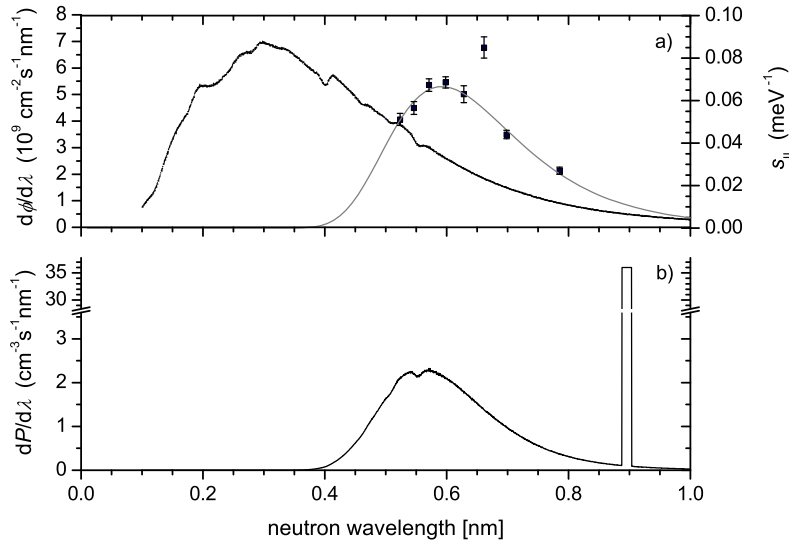


**Figure 6:** a) Differential flux at the neutron guide NL1 of FRMII (left scale), and measured scattering function  $s_{II}(\lambda)$  and fitted curve (right scale). The data point above the curve is due to the roton-maxon resonance in the multi-phonon dynamic structure factor. b) Calculated differential production rate, including single- and multi-phonon contributions, employing the measured  $d\phi/d\lambda$  and the fit function for  $s_{II}(\lambda)$  from fig. 6 a).

## 213 5 Discussion and conclusions

214 Our experiments demonstrate the feasibility of a versatile, intense UCN source at a cold neutron  
 215 beam, providing UCN for experiments at room temperature. With the present prototype, at  
 216  $T = 0.82$  K and using a small extraction hole with area  $A = 2 \text{ cm}^2$ , about 60 % of the UCN  
 217 produced in the Fomblin grease-coated converter vessel reached the detector. Compared to our  
 218 previous experiment with the uncoated electropolished stainless steel converter vessel [22], the  
 219 count rates of accumulated UCN observed immediately after opening the UCN valve, and also  
 220 the integral UCN counts were almost a factor three higher, despite the lower Fermi potential of  
 221 the Fomblin wall coating. This increase of UCN output is due to longer storage time constants  
 222 and a faster passage of the UCN through the extraction hole. Values for  $\tau_A$  as derived from  
 223 eq.(2) can be compared to the gas-kinetic equation

$$\tau_A = \frac{4V}{vA}, \quad (13)$$

224 where we insert  $V \approx 2.4$  l for the volume of the converter vessel, and the mean velocity  $v$  of the  
 225 trapped UCN, which, for a uniform distribution in velocity space, is given by  $v = 3v_{\text{max}}/4$  with  
 226  $m_n v_{\text{max}}^2/2 = V_{F,\text{wall}} - V_{F,^4\text{He}}$ , where  $m_n$  is the neutron mass. From the data for the Fomblin-  
 227 coated vessel at  $T = 1.26$  K we thus expect  $\tau_A = 14.8$  s. The measured value,  $\tau_A = (27 \pm 3)$  s, is  
 228 much closer to the expected value than in our earlier experiments with the uncoated converter  
 229 vessel. There, from eq.(13) with the Fermi potential of stainless steel we may expect  $\tau_A = 11.3$  s  
 230 but measured  $\tau_A = (58 \pm 13)$  s. A possible explanation is that UCN trajectories do not explore  
 231 quickly enough the available phase space in the electropolished vessel, a hypothesis already  
 232 raised earlier by W. Mampe and co-workers for their liquid-wall UCN bottle experiment [31].  
 233 Thus a certain roughness of the vessel walls seems to be necessary for efficient extraction of the  
 234 UCN through a small hole. This should be taken into account in the design of a large converter

235 vessel in order to keep the time needed to extract the UCN reasonably short.

236 The UCN production rate densities determined with two partly independent methods agree  
237 very well,  $\varepsilon P_1 = (0.80 \pm 0.08) \text{ s}^{-1}\text{cm}^{-3}$ , and  $\varepsilon P_2 = (0.79 \pm 0.09) \text{ s}^{-1}\text{cm}^{-3}$ . In our earlier  
238 experiment with the uncoated stainless steel vessel, we obtained the values  $\varepsilon P_1 = (0.91 \pm 0.21)$   
239  $\text{ s}^{-1}\text{cm}^{-3}$ , and  $\varepsilon P_2 = (1.09 \pm 0.25) \text{ s}^{-1}\text{cm}^{-3}$ . The accuracy of the comparison has thus been  
240 improved by more than a factor two in the present experiments. More important, also the  
241 comparison with the theoretical expectation has been improved by virtue of a dedicated TOF  
242 analysis of the cold neutron beam spectrum, due to which we may expect the UCN production  
243 rate density  $P_{\text{th}} = (1.17 \pm 0.17) \text{ s}^{-1}\text{cm}^{-3}$ , with single- and multi-phonon contributions of similar  
244 size. Since the detector and extraction efficiencies, expressed by the factor  $\varepsilon$ , cannot be expected  
245 as perfect, the measured values come indeed very close to  $P_{\text{th}}$ .

246 In the present experiments the saturated UCN density, normalised to the production volume  
247  $V_p$  did not exceed 46 UCN per  $\text{cm}^3$ . To avoid activation of the stainless steel vessel only a quarter  
248 of the total volume was irradiated with the cold beam. Also for practical reasons, significant  
249 divergence losses due to beam collimation were accepted. In addition, for simplicity of these  
250 first tests, we did not yet employ a wall material with low neutron absorption and a high Fermi  
251 potential of 250 neV or beyond, such as Be, BeO or diamond-like carbon [32, 33]. There one will  
252 gain in UCN density both due to the larger energy of the storable neutrons and due to a larger  
253 storage time. In order to produce a larger total number of UCN, the converter vessel can be  
254 made much longer, due to the low cross section of  $27 \times 10^{-27} \text{ cm}^2$  for neutrons with wavelength  
255 0.89 nm [34], corresponding to a mean free path of about 17 m. With a properly designed  $^4\text{He}$   
256 converter and using an existing intense cold neutron beam at a high flux reactor, UCN densities  
257 in the order  $10^4$  per  $\text{cm}^3$  with a total UCN number up to several  $10^8$  seem within reach.

258 **Acknowledgements:** We are very grateful to the head of the Physics Department E18,  
259 Prof. S. Paul, and to the scientific director of the FRM II, Prof. W. Petry, for supporting this  
260 development. We also thank I. Altarev, A. Müller and W. Schott for some useful discussions.  
261 We gratefully acknowledge the help of M. Pfaller and his team from the central mechanical  
262 workshop of the physics faculty for careful manufacturing of many cryostat components. This  
263 work has been funded by the German BMBF (contract number 06MT250).

## 264 References

- 265 [1] R. Golub, D. Richardson, S.K. Lamoreaux, *Ultra-Cold Neutrons*, IOP Publishing Ltd, 1991.
- 266 [2] V.K. Ignatovich, *The Physics of Ultracold Neutrons*, Clarendon Press, Oxford 1990.
- 267 [3] C.A. Baker et al., Phys. Rev. Lett **97** (2006) 131801.
- 268 [4] M. Pospelov, A. Ritz, Annals Phys. **318** (2005) 119.
- 269 [5] R.E. Lopez, M.S. Turner, Phys. Rev. D **59** (1999) 103502.
- 270 [6] M. Arif et al. (Eds.), Precision Measurements with Slow Neutrons, J. Res. Nat. Stand.  
271 Technol. **110** (2005) 137.
- 272 [7] H. Abele and D. Mund (Eds.), workshop on Quark mixing and CKM Unitarity, Heidelberg,  
273 September 2002 (Mattes Verlag, Heidelberg, 2003) [arXiv: hep-ph/0312124].
- 274 [8] V.V. Nesvizhevsky, H.G. Börner, A.K. Petukhov, H. Abele et al., Nature **415** (2002) 297.
- 275 [9] G. Ban, K. Bodek, M. Daum, R. Henneck et al., Phys. Rev. Lett. **99** (2007) 161603.

- 276 [10] A.P. Serebrov, E.B. Aleksandrov, N.A. Dovator, S.P. Dmitriev et al., submitted to Phys.  
277 Lett. B [arXiv:0706.3600].
- 278 [11] A. Steyerl, H. Nagel, F.-X. Schreiber et al., Phys. Lett. A **116** (1986) 347.
- 279 [12] U. Trinks, F.J. Hartmann, S. Paul, W. Schott, Nucl. Instr. Meth. A **440** (2000) 666.
- 280 [13] A. Fomin et al., PSI Report TM-00-14-01 (2000), see also <http://ucn.web.psi.ch/>.
- 281 [14] A. Saunders, J.M. Anaya, T.J. Bowles et al., Phys. Lett B **593** (2004) 55.
- 282 [15] Y.N. Pokotilovski, Nucl. Instr. Meth A **356** (1995) 412.
- 283 [16] Y. Masuda, T. Kitagaki, K. Hatanaka et al., Phys. Rev. Lett. **89** (2002) 284801-1.
- 284 [17] C.A. Baker, S.N. Balashov, J. Butterworth, P. Geltenbort et al., Phys. Lett. A **308** (2003)  
285 67.
- 286 [18] The LANSCE neutron EDM experiment, <http://p25ext.lanl.gov/edm/edm.html>.
- 287 [19] R. Golub and J.M. Pendlebury, Phys. Lett. **53A** (1975) 133.
- 288 [20] E. Korobkina, R. Golub, B.W. Wehring, A.R. Young, Phys. Lett. A **301** (2003) 462.
- 289 [21] W. Schott, J.M. Pendlebury, I. Altarev, S. Gröger et al., Eur. Phys. J. A **16** (2003) 599.
- 290 [22] O. Zimmer, K. Baumann, M. Fertl, B. Franke, S. Mironov, C. Plonka, D. Rich, P. Schmidt-  
291 Wellenburg, H.-F. Wirth, B. van den Brandt, Phys. Rev. Lett. **99** (2007) 104801.
- 292 [23] P.R. Huffman, C.R. Brome, J.S. Butterworth, K.J. Coakley et al., Nature **403** (2000) 62.
- 293 [24] P. Ageron, W. Mampe, R. Golub, J.M. Pendlebury, Phys. Lett. **66A** (1978) 469.
- 294 [25] H. Yoshiki, K. Sakai, T. Kawai, S. Goto'o, Cryogenics **34** (1994) 277.
- 295 [26] A.I. Kilvington et al., Phys. Lett. A **125** (1987) 416.
- 296 [27] K. Zeitelhack, C. Schanzer, A. Kastenmüller et al., Nucl. Instr. Meth. A **560** (2006) 444.
- 297 [28] K.H. Andersen, W.G. Stirling, R. Scherm, A. Stunault et al., J. Phys.: Condens. Matter **6**  
298 (1994) 821.
- 299 [29] K.H. Anderson, private communication of unpublished results.
- 300 [30] M. van der Grinten, private communication.
- 301 [31] W. Mampe, P. Ageron, C. Bates, J.M. Pendlebury, A. Steyerl, Phys. Rev. Lett. **63** (1989)  
302 593.
- 303 [32] F. Atchison, B. Blau, M. Daum, P. Fierlinger et al., Phys. Lett. B **642** (2006) 24.
- 304 [33] F. Atchison, B. Blau, M. Daum, P. Fierlinger et al., Phys. Rev. C **74** (2006) 055501.
- 305 [34] H.S. Sommers, J.G. Dash, L. Goldstein, Phys. Rev. **97** (1955) 855.